Phase-sensitive neutron reflectometry measurements applied in the study of photovoltaic films

J. W. Kiel,[1,2] M. E. Mackay,[2,a)] B. J. Kirby,[3] B. B. Maranville,[3] and C. F. Majkrzak[3,a)]
[1]*Department of Chemical Engineering and Materials Science, Michigan State University, East Lansing, Michigan 48824, USA*
[2]*Department of Materials Science and Engineering, The University of Delaware, Newark, Delaware 19716, USA*
[3]*National Institute of Standards and Technology Center for Neutron Scattering, Gaithersburg, Maryland 20899, USA*

(Received 4 May 2010; accepted 5 July 2010; published online 20 August 2010)

Due to low charge carrier mobilities in polymer-based solar cells, device performance is dictated by the nanoscale morphology of the active layer components. However, their morphological details are notoriously difficult to distinguish due to the low electron contrast difference between the components. Phase-sensitive neutron reflectivity (PSNR) is uniquely suited to characterize these systems due to the large, natural scattering length density difference between two common device materials, poly(3-hexylthiophene) and [6,6]-phenyl-C61-butyric acid methyl ester (PCBM). Using PSNR we find a high concentration of PCBM at the substrate and near but not at the air interface. Herein we discuss the method of applying PSNR to polymer-based solar cells, the results obtained, and an evaluation of its effectiveness. © *2010 American Institute of Physics*.
[doi:10.1063/1.3471583]

I. INTRODUCTION

Polymer-based solar cells have the potential to supplement the ever increasing societal energy demands in a cost effective manner due to their low cost and ease of manufacture. The device components are readily available and are typically a light absorbing polymer and a C_{60} fullerene derivative. However, commercialization will not be feasible until device performance reaches an efficiency level approaching that of inorganic cells, ~10%.[1] Achieving this level of performance is challenging as it requires control of the nanoscale morphology of a roughly 100 nm thick film of the polymer/nanoparticle active layer.

In traditional, inorganic solar cells photogenerated excitons are almost immediately separated into their component charge carriers because of the high dielectric constant of the inorganic material and the electric field created through doping. Polymers have low dielectric constants resulting in strong Coulombic interactions of the photogenerated excitons, dictating exciton diffusion lengths of the order of 5–10 nm.[2] Such a small length requires the exciton to be created within a short range of a dissociation point, the polymer/fullerene interface, to break into its components and generate free charge carriers. Otherwise it rapidly recombines and produces useless heat or light.

Coupling the exciton diffusion length with an appropriate device thickness to maximize light absorption requires the film morphology to be optimized on different lengths scales. The smaller exciton diffusion length requires the system to have polymer rich regions of the order of 10 nm wide, but a roughly 100 nm thickness is required to maximize light absorption based on the material's absorptivity. This places strict requirements on the internal morphology with an ideal device having polymer strands 10 nm wide and 100 nm long sandwiched between fullerene regions in a cocontinuous manner allowing both phases direct access to the appropriate electrode.[1]

This morphology must be developed in simple processing steps otherwise the rationale promoting this energy source is defunct. However, a full morphological description of the bulk heterojunction has yet to be developed because morphological characterization is challenging due to the small size scale and limited electron contrast between the polymer and nanoparticle. Robust relationships combining processing, morphology, and performance need to be developed to guide device manufacture. In our previous study[3] we demonstrated neutron scattering, in particular neutron reflectometery, is a most effective technique to characterize polymer/fullerene blends since there is a natural contrast in scattering potential among the constituent components, with no chemical modification of the components required. Here we describe the technique in detail and present results to aid development of more efficient devices by measuring morphology as a function of processing conditions.

Previously, improved device performance in these types of solar cells involved much experimentation by empirically changing material properties such as polymer regioregularity and molecular weight,[4] as well as fabrication variables such as solvent choice,[5] spin coating times,[6] and annealing.[7] All of these processing conditions have been shown to relate directly to the crystallinity of the polymer component of the

a)Authors to whom correspondence should be addressed. Electronic addresses: mem@udel.edu and charles.majkrzak@nist.gov.

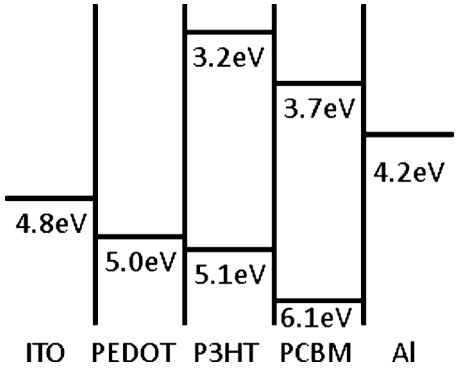

FIG. 1. Idealized energy diagram of a P3HT/PCBM solar cell, showing ideal alignment of the molecular orbitals, has the PCBM component of the cell in contact with the aluminum electrode and the P3HT component in contact with the hole conducting layer of PEDOT/PSS.

cell,[6] where improved polymer crystallinity provides greater hole mobilities through the structure, thereby improving device performance.[8]

While improved crystallinity and the corresponding hole transport properties are crucial, other factors certainly affect their performance. Traditional polymer-based solar cells are spin coated or printed from solution providing an undefined and kinetically trapped mixture of nanoparticles and polymer. The vast majority of these devices today are created from solutions containing a roughly 1:1 by weight mixture of polymer and nanoparticle. Yaklin *et al.* showed that C_{60} could be soluble in polystyrene thin films up to roughly 2% by volume,[9] but this required substantial manipulation of the films. While PCBM is more soluble then pure C_{60}, at such a high concentration in polymer-based solar cells, roughly 47% by volume, it is unlikely that the polymer and nanoparticle are completely soluble with each other, making a homogenous dispersion of the two components very unlikely.

Here we use a mixture of poly(3-hexylthiophene) (P3HT) and [6,6]-phenyl-C_{61}-butyric acid methyl ester (PCBM) as a standard system to study polymer-based solar cells. As seen in the energy diagram of an idealized P3HT/PCBM cell, Fig. 1, good electrical transport out of the cell only occurs if there is PCBM at the metal electrode and P3HT at the transparent indium tin oxide (ITO) electrode. Based on the ideal energy diagram and the short exciton diffusion length, a comblike structure would be ideal,[1] but this structure would be extremely difficult to make requiring lithographic methods that would eliminate the potential cost benefits of solution processable devices. To maintain the fabrication and cost benefits of solution processable devices, a casting or printing method seems inevitable, but determining the PCBM concentration profile within the devices has proven difficult.

Much work has gone into determining the morphology and concentration profile within these devices yielding different and contradictory results. Transmission electron microscopy (TEM), both defocused TEM[10] and electron tomography,[11] ellipsometry,[12,13] x-ray reflectivity,[14] and scanning electron microscopy[15] have all been used to investigate the vertical distribution of PCBM within the polymer active layer. The electron and x-ray techniques suffer from low contrast between the components since they are based on scattering from atomic electron clouds and the majority of the film is carbon. Using a density of 1.3 g/ml for PCBM[3] and a density of 1.1 g/ml for P3HT[16] we calculate the electron densities of each component; 4.0×10^{23} e^-/ml for PCBM and 3.6×10^{23} e^-/ml for P3HT, giving only about 5% contrast between the two components. Here we define contrast as the difference of the electron densities divided by their sum. With such weak contrast, distinguishing between the polymer and nanoparticle components is exceedingly difficult, hampering efforts to characterize morphological features. Ellipsometry, which uses refractive index and extinction coefficient profiles, has better sensitivity to differences in the two components, and in principle can be used to characterize the nanoparticle concentration profile. The anisotropic refractive index of P3HT makes modeling difficult, but recent work[13] shows comparable results to our reflectivity data indicating spectroscopic ellipsometry can be a practical, although modeling intensive, method for characterizing such films.

X-ray photoelectron spectroscopy[17] (XPS) and near edge x-ray absorption fine structure spectroscopy (NEXAFS)[18] results, which use electron orbitals and band structure to determine elemental compositions, show high concentrations of PCBM at an SiO_2 substrate directly after spin coating. These methods are an excellent way to characterize compositions near the surface of films, and the results in Refs. 17 and 18 are consistent with the results discussed here. However, XPS and NEXAFS cannot be used to determine depth profiles and are not sensitive to internal device structure.

II. EXPERIMENTAL PRELIMINARIES

A. Neutron reflectometry

For a specular neutron reflectometry measurement, the intensity of the reflected beam, R, is measured as a function of scattering vector, $Q=4\pi/\lambda \sin(\theta/2)$, where θ is the scattering angle and λ is the neutron wavelength. R(Q) is a function of the depth (z direction) dependent scattering potential of the thin film sample, which is commonly expressed in terms of scattering length density, $\rho(z)=[\Sigma_i b_i(z)/V_m]$, where the summation is over each type of isotope in the sample, b is the nuclear scattering length, and V_m is the molecular volume (the molecular weight divided by the mass density and Avogadro's number). Since b is a known quantity characteristic of a given isotope, neutron reflectometry can be used to characterize the average composition of a thin film as a function of depth into the film. Here we used neutron reflectometry to investigate solar cell mimics consisting of the polymer, P3HT, and the nanoparticle, PCBM, in a 1:1 by weight ratio in order to compare with many previous studies.[12,13,17,18] From the densities mentioned above, the component scattering length densities are found to be 3.76×10^{-6} and 0.67×10^{-6} A^{-2} for PCBM and P3HT, respectively, a contrast of 70%. These values were also verified experimentally by performing specular reflectivity on films of each pure component as discussed below.

Analysis of neutron reflectivity data can be complicated by not always providing a unique solution. One $\rho(z)$ profile

can produce one unique set of reflectivity data but the inverse is generally not true.[19] This situation arises from the total loss of phase information that occurs from measuring the reflectivity which is the *square* of the absolute magnitude of the scattered neutron's complex reflection amplitude ($R=|r|^2$). This loss in phase information results in one set of reflectivity data being able to produce multiple $\rho(z)$ profiles during fitting. Additionally, when fitting with the Parratt formalism[20] a least-squares minimization is used to determine an overall profile, which can provide multiple "correct" solutions to the data of films more complex than those consisting of only pure components. While retaining the phase information in one experiment is not possible, the phase information can be retrieved by varying the surrounding media during multiple reflectivity experiments.[21,22]

Phase-sensitive neutron reflectometry (PSNR) methods make it possible, through the use of variable reference films or substrates, to uniquely determine the complex reflection amplitude of an adjacent, "unknown," layered structure. This, in turn, can be directly inverted to yield its corresponding, unambiguous profile. An accessible review of neutron reflectometry (NR) techniques in general, and PSNR in particular, is given by Berk and co-workers.[23] There are two categories of references applicable in PSNR, layers of finite thickness with variable $\rho(z)$ [21,24] or surrounding media[22] of adjustable $\rho(z)$, i.e., either the "fronting" medium containing the incident and reflected waves, or the "backing" medium containing the transmitted. Either the fronting or backing medium may serve as the supporting substrate for a thin film system of interest. The variation of an *adjacent* reference layer or substrate in this way fundamentally differs from changing the contrast of a specific component *within* the layers of interest for the purpose of accentuating that feature. The ultimate sensitivity is achieved by performing phase-sensitive NR measurements for each of a number of different labelings of a component part.

B. Experimental objectives

Three principal goals for these phase-sensitive neutron reflectivity measurements were defined: (1) determining a unique $\rho(z)$ profile for the solar cell mimic films, (2) establishing the in-plane homogeneity of the films, and (3) ascertaining the effects of truncating the reflectivity data at a finite wave vector value (Q_{max}). These goals stem from the difficulties in determining the correct PCBM profile from the single neutron measurements performed in air and the possibility of having an inhomogeneous film.

A unique SLD depth profile can be obtained from specular reflectivity measurements only if any existing in-plane inhomogeneities of the SLD are on a sufficiently short length scale that the neutron wave packet effectively averages over the variations. For example, if a film has two or more distinct, in-plane regions of different SLD which are larger than the area an incident neutron wave packet projects on to, then the measured reflectivity will consist of an area-weighted, incoherent sum of reflectivities, where each independent component of the sum corresponds to one of the distinct regions. This resulting incoherent sum of reflectivities has no associated single SLD depth profile that is physically meaningful. If, on the other hand, the projection of the neutron wave onto the surface extends sufficiently over all regions of different in-plane SLD simultaneously, then the coherently reflected wave can be associated with a SLD that is the in-plane average. The presence of regions of different in-plane SLD of area greater than that which the neutron can effectively average over can be identified by a distortion of the form of the imaginary part of the reflection amplitude (which can be determined in phase-sensitive neutron reflectivity measurements).[19] For the instrumental configuration used in these reflectivity measurements, the effective area of the neutron wavepacket projected onto the surface is of the order of 100 μm.

Due to time constraints and signal-to-noise ratios, the reflectivity data must be truncated at some finite value of the wave vector, Q_{max}. Evaluation of truncation at some Q_{max} will determine the effective spatial resolution of the SLD depth profile and to what extent artifacts are introduced as a consequence of the cutoff. For the samples studied here the maximum practical value of Q obtainable is dictated primarily by signal-to-noise ratio rather than counting time alone and is more than adequate to uniquely characterize the concentration profile within the solar cell mimics we chose to study. As will be demonstrated in the following sections, we believe that, to a high degree of confidence, all of the above goals have been achieved.

III. EXPERIMENTAL SECTION

A. Sample preparation

To make the PSNR samples, both P3HT and PCBM were weighed out in a 1:1 by weight ratio in air. The polymer/nanoparticle mixture was then transferred to a nitrogen glove box and chlorobenzene was added such that a total solution concentration of 30 mg/ml was obtained (15 mg P3HT and 15 mg PCBM per 1 ml of solvent). The solution was stirred for three days inside the glove box and then filtered through a 200 nm PTFE filter. Two samples for the PSNR tests were spin coated onto 75.2 mm diameter, 5 mm thick polished silicon slabs; one at 2500 RPMs for 60 s, denoted "fast grown" and one at 800 RPMs for 180 s, denoted "slow grown." The solution was first heated to 50 °C before spin coating for the slow grown sample to achieve a completely flat film. Visual inspection of both of these unannealed samples showed minor defects, the total defect area amounting to a relatively small fraction of the total area illuminated by the incident neutron beam. Thus, based on this optical criterion, these two samples were deemed to be of potentially sufficient in-plane homogeneity to warrant further study by PSNR. Such was not the case for some films annealed at 140 °C for 10 min as we found large agglomerates of PCBM formed upon thermal annealing, similar to previous reports.[12]

The pure P3HT and PCBM samples were created following the same weighing procedure using only pure components. Pure P3HT samples were spin coated at 2500 RPMs and the pure PCBM was spin coated at 2000 RPM, both at a concentration of 20 mg/ml in chlorobenzene. In this case

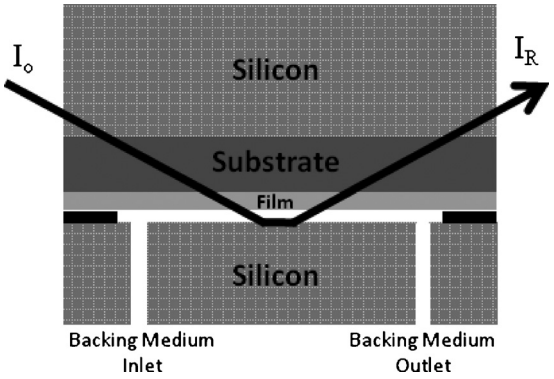

FIG. 2. A cross sectional image of the wet cell holder used for phase-sensitive neutron reflectivity measurements. The path of the neutron beam enters through a silicon "fronting," encounters the film being studied and exits through to the "backing" reservoir, which was either air or D_2O for this experiment.

though the silicon wafers were 50.8 mm in diameter and 1 mm thick. The larger silicon slabs were not needed for these tests as the pure components did not require PSNR calculations nor the sample holder described below due to the low complexity of the films.

All samples were transported from the University of Delaware to NIST in a nitrogen filled vacuum dessicator to ensure no oxygen degradation. However, subsequent reflectivity measurements showed no change in reflectivity or extracted $\rho(z)$ profiles after many days exposure of the films to oxygen.

B. Phase-sensitive neutron reflectometry

PSNR measurements were performed on the NG1 polarized neutron reflectometer at NIST with an incident wavelength of 4.75 Å and a fractional standard deviation of the wavelength of 0.01. A wet cell holder, Fig. 2, allowed for easy changing of the backing media. Wafers were inserted into the wet cell, aligned on the reflectometer, and data were taken with air as the backing media. After the air backing data was gathered, degassed D_2O was slowly injected into the wet cell as the new backing media and a new data set was taken. The reservoir thickness of the backing medium was approximately 100 μm, defined by a flat Viton gasket. No realigning was performed upon addition of the D_2O but rocking curves were periodically taken during the course of both the air and D_2O backing experiments to ensure no misalignment occurred.

The pair of composite system measurements for each of the two samples enabled determination of the complex reflection amplitude, both real and imaginary parts, as mentioned earlier. To verify that neither the sample film, e.g., by absorption of water from the reservoir, nor the water level of the reservoir itself changed over the course of the measurements, the reflectivity curves were repeated several times. In addition, transverse scans were periodically performed to monitor alignment as well as the constancy of the water level. In no case was a problem detected and all of the data collected are believed to be quantitatively accurate and precise to a few percent.

We note that the Si substrate for the fast grown sample was slightly distorted from perfect flatness, most likely due to the manufacturers polishing procedure, with a transverse or rocking curve width of approximately 0.034° FWHM, slightly larger than the instrumental resolution of 0.02° FWHM. The silicon substrate for the slow grown sample was flatter with a FWHM of approximately 0.21°. Deviation of the substrate from perfect flatness results in an effective degradation of the instrumental Q resolution perpendicular to the substrate surface, i.e., for the specular scan. The flatness discussed here refers to the length scale of approximately hundreds of microns, as opposed to the nanometer length scale associated with interfacial "roughness," typically quoted as an RMS value. For all of the measurements the slit apertures were opened with increasing Q, once sufficiently above the critical angle region, so as to maintain an approximately constant "footprint" of illumination on the sample surface. This footprint measured about 25 mm in height and 40 mm in length along the horizontal. Because of the large silicon substrates, 75.2 mm diameter, no footprint correction was needed for data reduction of the PSNR samples. A slight footprint adjustment was needed for the low Q values on the pure component samples because those measurements were taken on 50.8 mm diameter substrates. For all measurements, the fractional standard deviation of the wavevector transfer, dQ/Q, was kept approximately constant at 0.025.

The reflectivity was obtained by subtracting background from the measured reflected intensity and subsequently dividing by the incident intensity appropriate for the set of aperture widths at a given value of Q. Given the beam time available to us, it was possible to collect reflectivity data for the fast grown sample with both air and water references out to a Q of nearly 0.2 $Å^{-1}$. For the slow grown sample, it was possible to collect reflectivity data out to 0.2 $Å^{-1}$ for the D_2O backing but only to about 0.1 $Å^{-1}$ for the air backing.

Once the specular reflectivity data sets for the composite systems were obtained, two different analyses were performed to extract the $\rho(z)$ depth profiles of the films, which can be shown to be unique to within the extent allowed by the statistical uncertainty in the data and its truncation at some value of Q_{max}. The first analysis extracted the real and imaginary parts of the complex reflection amplitude corresponding to the "unknown" polymer film of interest (the scattering length density associated with fronting and backing media are automatically separated out in the process). The real part of the reflection amplitude was then mathematically inverted[25] to obtain the unique $\rho(z)$ profile of the film, using no adjustable parameters whatsoever. As a second method, the two composite system reflectivity data sets for each polymer film were simultaneously fitted, which can be shown to also lead to an unambiguous $\rho(z)$ profile since the phase information is contained in the two composite system reflectivity data sets.[26] In addition, the corresponding imaginary part of the reflection amplitude was obtained and examined to determine, at least semiquantitatively, the degree of in-plane homogeneity of the film, Fig. 6, on a length scale commensurate with the lateral coherence length of the incident neutrons.[19]

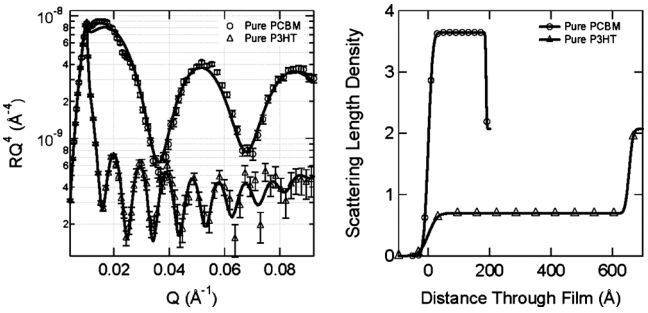

FIG. 3. (a) RQ^4 vs Q for pure films of P3HT (△) and PCBM (○) and (b) corresponding SLD profiles from the best fit lines of the data. The PCBM film (~23 nm) was noticeably thinner than the P3HT film (~69 nm) due to spin coating conditions. All fitting was performed using the Parratt formalism and both film profiles terminate at an SLD of 2.07×10^{-6} A^{-2}, that of the pure silicon substrate. The native SiO_2 layer is not seen in the P3HT film profile due to the film thickness and finite Q obtained. The PCBM film is small enough to see the SiO_2 layer, but it is contrast matched almost exactly and therefore blends into the PCBM SLD profile.

IV. RESULTS AND DISCUSSION

A. Pure component films

Figure 3 is reflectivity data plotted as RQ^4 versus Q with associated best fits to the data. The convention RQ^4 is used because reflectivity decreases at a rate of Q^{-4} for systems with sharp interfaces at high Q. As these films are pure components phase determination was deemed unnecessary and the data were fitted according to the Parratt formalism[20] using the program MOTOFIT,[27] giving values of 3.6×10^{-6} and 0.70×10^{-6} $Å^{-2}$ for PCBM and P3HT, respectively, values nearly identical to the calculated values.

With the pure component $\rho(z)$ profiles known we could begin to test and model solar cell mimics that contained both P3HT and PCBM. However, these films are both complex and unknown, at least in terms of nanoparticle dispersion, so fitting the $\rho(z)$ profile using the Parratt formalism[20] from one scattering experiment proved difficult. Multiple solutions could be obtained that showed reasonable thicknesses and theoretically possible $\rho(z)$ profiles that provided acceptable values of total PCBM and P3HT within the system (i.e., the mass balance was effectively conserved, showing roughly 48 vol % PCBM and 52 vol % P3HT). Determining which profile was indeed correct proved difficult as the previous studies mentioned above provided conflicting results. Hence, the phase-sensitive tests, described below, were performed.

B. Fast grown film

The composite reflectivity data sets obtained for the fast grown film and associated fits, which were determined simultaneously using the program GA_REFL developed by Kienzle *et al.*[28] at NIST, are shown in Fig. 4(a). The reflection amplitude corresponding to the polymer film alone, as extracted mathematically via the methods described in the literature cited earlier and the film $\rho(z)$ profiles obtained by simultaneous fitting and direct inversion of Re[r], are shown together in Figs. 4(b) and 4(c), respectively. The agreement of the $\rho(z)$ profiles is remarkable. What relatively minor differences are evident can be attributed to the statistical uncertainty in the data and its truncation at a finite, maximum Q.[29]

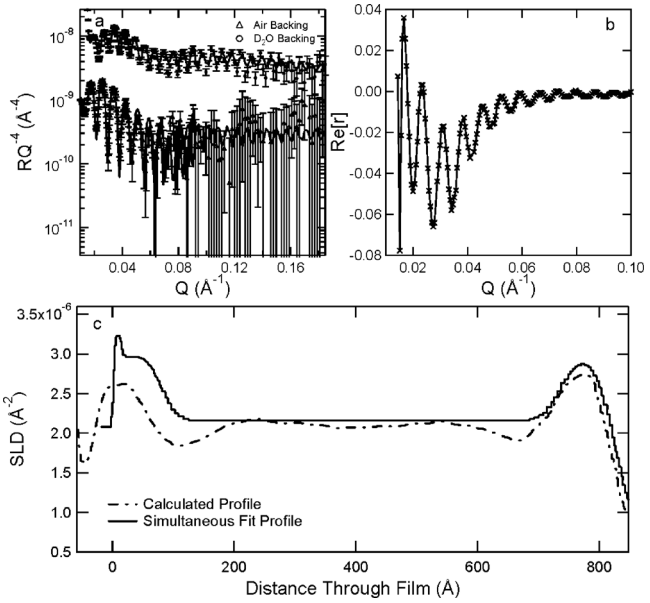

FIG. 4. Results for the fast grown film spin coated from a 1:1 mixture by weight of P3HT and PCBM in chlorobenzene spin coated at 2500 RPMs. (a) Composite reflectivity data sets obtained from specular reflectivity in both air and D_2O. Large error bars at high Q for the air sample are expected as the reflectance here is approaching the background. (b) The real part of the reflection amplitude corresponding to the film as extracted mathematically via the methods described in the text. (c) The fast grown film SLD profiles obtained by simultaneous fitting and direct inversion of Re[r] shown together.

The relatively sharp spike in SLD at the substrate/film interface in the simultaneous fit result was imposed on the profile independently to account for the SiO_2 passive layer typically found on bare silicon. Because of its relatively narrow width, this feature is not directly observable for reflectivity data collected up to the current Q_{max}. As discussed in greater detail in a previous work,[3] an increase in $\rho(z)$ is seen at the substrate and near, but not at the air interface.

PCBM concentration is directly related to the $\rho(z)$ and can be found using a simple equation

$$\phi_{PCBM} = \frac{\rho(z) - \rho_{P3HT}}{\rho_{PCBM} - \rho_{P3HT}}, \quad (1)$$

where ϕ_{PCBM} is the volume fraction of PCBM and ρ_{PCBM} and ρ_{P3HT} are the $\rho(z)$ of the two pure components determined in separate experiments (see Fig. 2). The maximum concentration of PCBM at the substrate and near the air interface is 74% and 65% by volume, respectively. A slight difference can be seen between the PSNR direct inversion technique and the simultaneous fitting, particularly near the substrate. These differences can be thought of as one gauge of the uncertainty in the profile and do not significantly diminish conclusions we can gather from this data. For example, the energy diagram, Fig. 1, indicates that PCBM should be at the air interface (the metal electrode) and not at the substrate (the conducting oxide). Clearly, both analysis techniques demonstrate that a high concentration of PCBM is present at undesirable locations.

For a variety of reasons these reflectometry measurements were performed on silicon wafers with a native oxide present instead of poly(3,4-ethylenedioxythiophene) poly-

(styrenesulfonate) (PEDOT:PSS) coated ITO slides, which are the traditional substrates for polymer-based solar cells. We note the substrate surface energy can affect the PCBM concentration profile, however, at present we cannot avoid its consequences, as discussed below. ITO coated glass slides have a substantial roughness, both on the nanometer and micron scales, making reflectivity measurements difficult. Additionally, gathering the PSNR composite data sets required flooding the top of each film with D_2O which dissolves the water soluble PEDOT:PSS layer. Although the PEDOT:PSS is coated with the hydrophobic active layer, we found that regardless of the care taken to make a perfect, defect free film the D_2O always diffused through or around the active layer into the PEDOT:PSS, swelling it and rendering the data and the film worthless. Hence no PEDOT:PSS layer was used.

As discussed earlier, the imaginary part of the reflection amplitude for the film as a function of wave vector, Im[r](Q), is sensitive to in-plane inhomogeneities. Im[r] for the fast grown film showed no obvious indication of any such density variation on a length scale of the order of 100 μm. A plot of Im[r](Q) for the slow grown film indicated a similar degree of homogeneity and is plotted for illustration purposes in the next section.

C. Slow grown film

The composite reflectivity data sets obtained for the slow grown film and fits, which were determined simultaneously, and the associated SLD profiles are shown in Figs. 5(a) and 5(b). Though noisier than that for the fast grown film, because composite system reflectivity data next to air were collected only out to approximately half the maximum Q due to beam time limitations, the SLD profile obtained via inversion of Re[r] is in good agreement with the dual fitting. The imaginary part of the reflection amplitude Im[r](Q) for the slow grown film, which is sensitive to in-plane inhomogeneities on a length scale of the order of 100 μm, is plotted in Fig. 6. The presence of well-defined zero crossing points between the two roots of the quadratic equation for Im[r] (one root corresponds to the actual physical solution) is indicative of effective coherent averaging by the neutron wave on a length scale of the order of its lateral coherence length.[19]

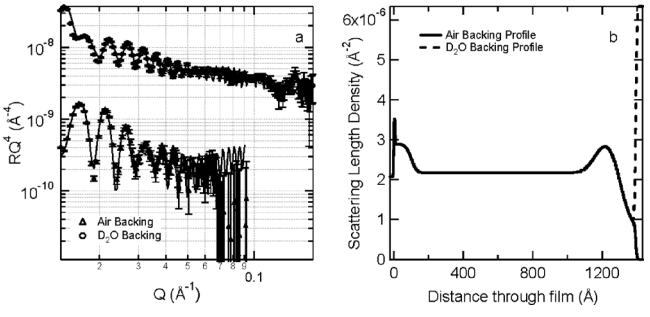

FIG. 5. (a) Composite reflectivity data sets obtained for the slow grown film and fits which were determined simultaneously and (b) the slow grown film SLD profile obtained by simultaneous fitting of the corresponding data. As the SLD profiles were simultaneously fitted the profiles overlap until the backing layer was reached and they differ with the air backing film going to SLD=0×10^{-6} Å^{-2} and the D_2O backing film going to an SLD=6.2×10^{-6} Å^{-2}.

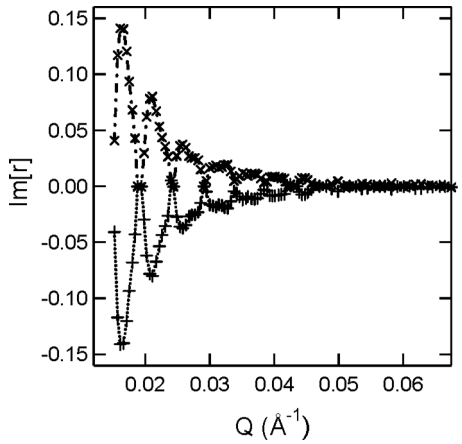

FIG. 6. The imaginary part of the reflection amplitude for the film in Fig. 5, Im[r](q), which is sensitive to in-plane inhomogeneities on a length scale of the order of a hundred microns. The presence of well-defined zero crossing points indicates a very homogeneous and good film.

D. Effects of reflectivity data truncation

Finally, in this section, we address one other key issue: whether truncation of neutron reflectivity data, at a finite maximum wave vector transfer Q_{max}, introduces "ringing" artifacts in the extracted scattering length density profile which might be misinterpreted as evidence of excess PCBM concentration at the interfaces.

To answer this question, two model scattering length density $\rho(z)$ profiles were investigated [Fig. 7(a)]. Each profile extends 900 Å, one having peaked structures adjacent to both interfaces, closely mimicking that which was obtained in the experiment, the other a single homogeneous slab with a constant $\rho(z)$ equal to the average of the former profile. The real part of the reflection amplitude was calculated for each of the model $\rho(z)$ profiles described above and then inverted using the exact one-dimensional quantum mechanical theory, but for limited ranges of Re[r], in one case up to $Q_{max}=0.4$ Å^{-1} and in another up to only 0.1 Å^{-1}. Figure

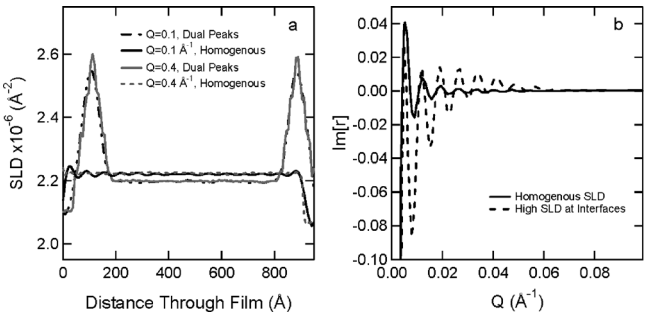

FIG. 7. (a) SLD profiles obtained by inverting the real part of the reflection amplitude generated from the two model profiles, one flat and homogeneous and the other with increased SLD at the interfaces. (b) Imaginary part of the reflection amplitude, Im[r] (corresponding to Re[r]), for the two profiles, i.e., the flat homogeneous case (solid line) and the one with increased SLD adjacent to the interfaces (dashed line).

7(b) is a plot of Im[r] for the two profiles, i.e., the flat homogeneous case and the one with increased $\rho(z)$ adjacent to the interfaces.

As indicated in Fig. 7, the scattering from the two structures is significantly different from one another, at least as is manifested in the imaginary part of the reflection amplitude, retrieved using phase-sensitive neutron reflection methods indicating there is substantial difference in scattering results between a homogenous film and one with PCBM concentrated at both interfaces. Comparison of the $\rho(z)$ profiles obtained by inverting the real part of the reflection amplitude generated from the two model profiles is shown in Fig. 7(a). Two inversions were performed for each model profile, one for Re[r](Q) values up to $Q_{max}=0.4$ Å^{-1}, the other for $Q_{max}=0.1$ Å^{-1}. In all cases, the oscillation or ringing which arises as an artifact of the truncation of Re[r] at finite Q is negligible in comparison to the size of the actual enhanced SLD values adjacent to the interfaces.[29]

The phase-sensitive neutron reflectivity methods, applied both to measurements on actual photovoltaic films as well to representative model $\rho(z)$ profiles, demonstrate that the effects of truncating reflectivity data at finite maximum values of wave vector transfer do not introduce spurious effects of sufficient magnitude to cause any significant misinterpretation in regard to the actual enhanced scattering length density in the vicinity of either interface.

V. CONCLUSION

Several important conclusions can be drawn from these phase-sensitive neutron reflectivity measurements on unannealed photovoltaic films containing the polymer P3HT and PCBM nanoparticles. First, the in-plane density distribution of matter across the plane of the film is of sufficient homogeneity to ensure adequate coherent averaging of the neutron wave—which is a prerequisite for a meaningful correlation of specular neutron reflectivity data with a single, representative $\rho(z)$ depth profile across the thickness of the film. Second, the unique $\rho(z)$ profiles retrieved from phase-sensitive neutron reflectivity data reveal an unambiguous concentration of PCBM at the substrate/film and film/air interfaces. That is, it conclusively shows the fullerene derivatives contained in the film are not distributed uniformly but, rather, are more concentrated at the two interfaces. Finally, PSNR measurements and analysis demonstrate that the effects of truncating reflectivity data at the finite maximum values of Q reached in the present studies do not introduce spurious effects of sufficient magnitude to cause any significant misinterpretation in regard to the actual enhanced scattering length density in the vicinity of either interface.

ACKNOWLEDGMENTS

This work was primarily supported by NSF Grant No. NIRT-0506309 and partially supported by the U.S. Department of Energy under research Contract No. DE-FG02-05ER46211. In addition, funding from the Center for Neutron Science at the University of Delaware is greatly appreciated. Commercial materials, instruments, and equipment are identified in this paper to specify the experimental procedure as completely as possible. In no case does such identification imply a recommendation or endorsement by the National Institute of Standards and Technology nor does it imply that the materials, instruments, or equipment identified are necessarily the best available for the purpose.

[1] K. M. Coakley and M. D. McGehee, Chem. Mater. **16**, 4533 (2004).
[2] D. E. Markov, E. Amsterdam, P. W. M. Blom, A. B. Sieval, and J. C. Hummelen, J. Phys. Chem. A **109**, 5266 (2005).
[3] J. W. Kiel, B. J. Kirby, C. F. Majkrzak, B. B. Maranville, and M. E. Mackay, Soft Matter **6**, 641 (2010).
[4] R. J. Kline, M. D. McGehee, E. N. Kadnikova, J. S. Liu, J. M. J. Frechet, and M. F. Toney, Macromolecules **38**, 3312 (2005).
[5] C. J. Brabec, N. S. Sariciftci, and J. C. Hummelen, Adv. Funct. Mater. **11**, 15 (2001).
[6] G. Li, Y. Yao, H. Yang, V. Shrotriya, G. Yang, and Y. Yang, Adv. Funct. Mater. **17**, 1636 (2007).
[7] G. Li, V. Shrotriya, Y. Yao, and Y. Yang, J. Appl. Phys. **98**, 043704 (2005).
[8] G. Li, V. Shrotriya, J. S. Huang, Y. Yao, T. Moriarty, K. Emery, and Y. Yang, Nature Mater. **4**, 864 (2005).
[9] M. A. Yaklin, P. M. Duxbury, and M. E. Mackay, Soft Matter **4**, 2441 (2008).
[10] J. S. Moon, J. K. Lee, S. N. Cho, J. Y. Byun, and A. J. Heeger, Nano Lett. **9**, 230 (2009).
[11] S. S. van Bavel, E. Sourty, G. de With, and J. Loos, Nano Lett. **9**, 507 (2009).
[12] M. Campoy-Quiles, T. Ferenczi, T. Agostinelli, P. G. Etchegoin, Y. Kim, T. D. Anthopoulos, P. N. Stavrinou, D. D. C. Bradley, and J. Nelson, Nature Mater. **7**, 158 (2008).
[13] D. S. Germack, C. K. Chan, R. J. Kline, D. A. Fischer, D. J. Gundlach, M. F. Toney, L. J. Richter, and D. M. DeLongchamp, Macromolecules **43**, 3828 (2010).
[14] J. W. Andreasen, S. A. Gevorgyan, C. M. Schleputz, and F. C. Krebs, Sol. Energy Mater. Sol. Cells **92**, 793 (2008).
[15] H. Hoppe, M. Niggemann, C. Winder, J. Kraut, R. Hiesgen, A. Hinsch, D. Meissner, and N. S. Sariciftci, Adv. Funct. Mater. **14**, 1005 (2004).
[16] T. J. Prosa, M. J. Winokur, J. Moulton, P. Smith, and A. J. Heeger, Macromolecules **25**, 4364 (1992).
[17] Z. Xu, L. M. Chen, G. Yang, C. H. Huang, J. Hou, Y. Wu, G. Li, C. S. Hsu, and Y. Yang, Adv. Funct. Mater. **19**, 1227 (2009).
[18] D. S. Germack, C. K. Chan, B. H. Hamadani, L. J. Richter, D. A. Fischer, D. J. Gundlach, and D. M. DeLongchamp, Appl. Phys. Lett. **94**, 233303 (2009).
[19] C. F. Majkrzak, N. F. Berk, V. Silin, and C. W. Meuse, Physica B **283**, 248 (2000).
[20] L. G. Parratt, Phys. Rev. **95**, 359 (1954).
[21] C. F. Majkrzak and N. F. Berk, Phys. Rev. B **52**, 10827 (1995).
[22] C. F. Majkrzak and N. F. Berk, Phys. Rev. B **58**, 15416 (1998).
[23] C. F. Majkrzak, N. F. Berk, and U. A. Perez-Salas, Langmuir **19**, 7796 (2003).
[24] V. O. de Haan, A. A. Vanwell, S. Adenwalla, and G. P. Felcher, Phys. Rev. B **52**, 10831 (1995).
[25] N. F. Berk and C. F. Majkrzak, J. Phys. Soc. Jpn. **65**, 107 (1996); K. Chadan and P. C. Sabattier, *Inverse Problems in Quantum Scattering Theory* (Springer-Verlag, New York, 1989); P. E. Sacks, Wave Motion **18**, 21 (1993).
[26] C. F. Majkrzak, N. F. Berk, P. Kienzle, and U. Perez-Salas, Langmuir **25**, 4154 (2009).
[27] A. Nelson, J. Appl. Crystallogr. **39**, 273 (2006).
[28] P. A. Kienzle, M. Doucet, D. J. McGillivray, K. V. O'Donovan, N. F. Berk, and C. F. Majkrzak, http://www.ncnr.nist.gov/reflpak, 2000–2006.
[29] N. F. Berk and C. F. Majkrzak, Langmuir **25**, 4132 (2009).